

# Implicit Neural Representation for MRI Parallel Imaging Reconstruction

Hao Li<sup>1\*</sup>, Yusheng Zhou<sup>2\*</sup>, Jianan Liu<sup>3\*\*</sup>, Xiling Liu<sup>4</sup>, Tao Huang<sup>5</sup>,  
Zhihan Lv<sup>6</sup>, and Weidong Cai<sup>7</sup>

<sup>1</sup> The Department of Neuroradiology, University Hospital Heidelberg,  
Heidelberg, Germany

<sup>2</sup> School of Electrical Engineering and Automation, Wuhan University, Wuhan, China

<sup>3</sup> Vitalent Consulting, Gothenburg, Sweden

<sup>4</sup> Department of Stomatology, Shenzhen People's Hospital, (The Second Clinical  
Medical College, Jinan University);

The First Affiliated Hospital, Southern University of Science and Technology)  
Shenzhen, China

<sup>5</sup> The College of Science and Engineering, James Cook University, Cairns, Australia

<sup>6</sup> Department of Game Design, Faculty of Arts, Uppsala University, Sweden

<sup>7</sup> School of Computer Science, University of Sydney, Sydney, Australia

**Abstract.** Magnetic resonance imaging (MRI) usually faces lengthy acquisition times, prompting the exploration of strategies such as parallel imaging (PI) to alleviate this problem by periodically skipping specific K-space lines and subsequently reconstructing high-quality images from the undersampled K-space. Implicit neural representation (INR) has recently emerged as a promising deep learning technique, characterizing objects as continuous functions of spatial coordinates typically parameterized by a multilayer perceptron (MLP). In this study, we propose a novel MRI PI reconstruction method that uses INR. Our approach represents reconstructed fully-sampled images as functions of voxel coordinates and prior feature vectors from undersampled images, addressing the generalization challenges of INR. Specifically, we introduce a scale-embedded encoder to generate scale-independent, voxel-specific features from MR images across various undersampling scales. These features are then concatenated with coordinate vectors to reconstruct fully-sampled MR images, facilitating multiple-scale reconstructions. To evaluate our method's performance, we conducted experiments using publicly available MRI datasets, comparing it with alternative reconstruction techniques. Our quantitative assessment demonstrates the superiority of our proposed method.

**Keywords:** Magnetic resonance imaging · parallel imaging reconstruction · implicit neural representation · supervised learning

---

\* Authors contribute equally to this work and are co-first authors.

\*\* Corresponding Author, Email: jianan.liu@vitalent.se.

## 1 Introduction

Magnetic resonance imaging (MRI) stands as a crucial non-ionizing medical imaging modality. However, a persistent challenge in MRI is the lengthy acquisition time. Strategies aimed at accelerating the speed of MRI acquisition while maintaining image fidelity involve omitting K-space lines in the phase-encoding direction, followed by reconstructing images from undersampled data. Notable methodologies addressing this challenge encompass compressed sensing (CS) [1] and parallel imaging (PI) [2,3]. PI is a commonly used technique to accelerate MRI scans by utilizing the redundancy present in multiple receiving coil elements to periodically reduce phase encoding steps. However, PI is prone to noise and aliasing artifacts, particularly at high undersampling factors.

Recent advances in MRI reconstruction have been driven by deep learning-based methods, categorized into data-driven and model-driven approaches [4]. Data-driven methods [5,6] train neural networks end-to-end to map undersampled MR images to fully-sampled ones. On the contrary, model-driven methods [7,8] adapt conventional iterative reconstruction algorithms using networks to learn auxiliary parameters or regularizations. While these approaches surpass conventional parallel imaging (PI) methods, a drawback is their reliance on fixed undersampling scales, necessitating separate training and storage for each scale, leading to high computational demands and resource utilization.

In recent years, implicit neural representation (INR) has gained traction in computer vision tasks, offering continuous function modeling of 2D slices or 3D volumes based on spatial coordinates [9,10]. In particular, the neural radiance field (NeRF) framework proposed by Mildenhall *et al.* [11] utilizes INR to render novel views with high visual quality. INR has also found application in medical imaging, including super-resolution techniques for MRI [12,13,14]. Methods such as NeRP [15] and NeSVoR [16] have shown promising results in reconstructing MRI images. Feng *et al.* [17] and Yang *et al.* [18] have proposed scan-specific methods based on INR for PI and CS reconstruction. However, a significant drawback of these methods is the need to train separate networks for each image slice/volume and each scale factor, resulting in long training times per subject [17], making it impractical for real clinical settings.

Building on previous INR-based approaches, we implemented INR for MRI PI reconstruction to mitigate generalization issues encountered in traditional INR methods, including subject-specific and undersampling factor-specific limitations. The main contributions of this paper are as follows.

- Proposing an implicit neural representation (INR) approach for representing fully-sampled MRI images as a continuous function of spatial coordinates and prior voxel-specific features from undersampled MRI data.
- A convolutional encoder network was introduced to extract voxel-specific features from undersampled MRI images, enhancing the recovery of voxel intensities without subject-specific constraints.
- Integration of a reconstruction scale within the encoder to produce uniform scale-independent features, enabling the recovery of MRI with multiple undersampling scales, even without explicit training.

- Experimental results demonstrate the superior performance and generation of high-quality images compared to other MRI PI reconstruction methods.

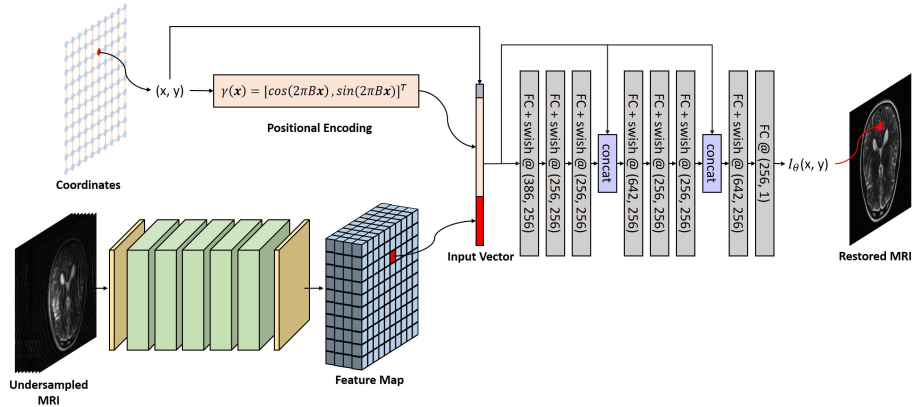


**Fig. 1.** The workflow of the proposed model is illustrated. The channel-wise undersampled images acquired by a multi-channel coil are converted into a feature map by a scale-embedded encoder. Simultaneously, the 2D voxel coordinates are transformed into higher-dimensional vectors. These feature and coordinate vectors are then concatenated at each coordinate and input into a multilayer perceptron (MLP) to recover voxel intensities at each corresponding coordinate to recover the fully-sampled image.

## 2 Methodology

### 2.1 Problem Formulation

For an MRI system, the undersampled k-space signal  $y$  can be expressed as:

$$y = \mathbf{A}I + \mathbf{n} \quad (1)$$

where  $I$  represents the image to be reconstructed and  $\mathbf{n}$  is the measurement noise.  $\mathbf{A} = \mathbf{M}\mathbf{F}$  denotes the degradation operator, where  $\mathbf{M}$  is a sampling mask, and  $\mathbf{F}$  denotes the Fourier transform. In previous MRI reconstruction studies, the image  $I$  is restored by minimizing the following objective function:

$$\operatorname{argmin}_I \frac{1}{2} \|y - \mathbf{A}I\|^2 \quad (2)$$

In INR, the MRI intensities  $I$  are regarded as a continuous coordinated-based implicit function, i.e.,  $f_\theta(\mathbf{x})$ , where  $\theta$  indicates the parameters of this function and  $\mathbf{x} = (x, y)$  denotes 2D voxel coordinates, which are normalized to the range

of  $[-1, 1]$ . Let  $I_\theta$  be the discretized image matrix after uniform sampling from  $f_\theta$  at the voxel locations. In this case, the reconstruction objective is rewritten as:

$$\operatorname{argmin}_\theta \frac{1}{2} \|y - \mathbf{A}I_\theta\|^2 \quad (3)$$

Based on implicit neural representation (INR),  $f_\theta$  is built as a multilayer perceptron (MLP), which has enlarged receptive fields with lower memory and time cost than convolutional neural networks [19]. Thus, this reconstruction problem is transformed into training a network to optimize function (3).

## 2.2 Arbitrary Scale Reconstruction

To improve the learning of high-frequency features, we adopt a positional encoding method from Tancik *et al.* [20]. The coordinates  $\mathbf{x} \in \mathbb{R}^2$  are transformed to a higher dimension space  $\mathbb{R}^{2L}$  using an encoding function  $\gamma$  before passing to the MLP:

$$\gamma(\mathbf{x}) = [\cos(2\pi B\mathbf{x}), \sin(2\pi B\mathbf{x})]^T \quad (4)$$

where  $B$  represents the encoding coefficients. All entries of the matrix  $B$  are sampled from the Gaussian distribution  $\mathcal{N}(\mathbf{0}, \sigma^2)$ , where  $\sigma$  is a tunable hyperparameter. In this work,  $\sigma$  is set to 1.

Training a specific function  $f_\theta$  for each undersampled image is impractical in clinical settings. Instead, a generic one is preferred. Towards this end, the prior intensity information of the undersampled images is used as an extra input of  $f_\theta$ , due to the lack of specificity of coordinates. We induce a convolutional encoder network to compress the local voxel intensity of the input images into a voxel-specific feature map  $V \in \mathbb{R}^{h \times w \times d}$ . Thus, each feature vector in the feature map denoted by  $v_{\mathbf{x}} \in \mathbb{R}^d$  contains the local semantic information of the MR image at the coordinate  $\mathbf{x}$ , which helps MLP recover the specific voxel intensity.

Furthermore, the undersampling scale of each MRI is not limited to a specific value in this recovery process, which means the implicit function  $f_\theta$  only learns the mapping from coordinates and feature vectors to voxel intensities. Thus, a reconstruction of multiple scale factors can be theoretically achieved. To enable the ability to discriminate different reconstruction scales and generate a uniform scale-independent feature map, we also embed the scale factor into the encoder.

$$v_{\mathbf{x}}^s = \operatorname{Encoder}(I_u^s, s)(\mathbf{x}) \quad (5)$$

where  $s$  is the reconstruction scale,  $I_u^s$  is the undersampled MR images with the reconstruction scale  $s$ , and  $v_{\mathbf{x}}^s$  denotes the prior feature vector of image  $I_u^s$  at the coordinate  $\mathbf{x}$ .

Finally, the implicit voxel function is:

$$I = f_\theta(\gamma(\mathbf{x}), v_{\mathbf{x}}^s) \quad (6)$$

$f_\theta$  and scale-embedded encoder are trained at the same time, and the MRI images with multiple undersampling scales can be reconstructed in a short time after the training.

Since all the operations mentioned above are conducted in the image domain, we modify the reconstruction objective for convenient training of all networks:

$$\operatorname{argmin}_{\theta} \frac{1}{2} \|I^* - I_{\theta}\|^2 \quad (7)$$

where  $I^*$  denotes the fully-sampled MR image.

### 2.3 Overall Framework

The overall framework of our method is illustrated in Fig. 1. The channel-wise undersampled images acquired by a multi-channel coil are converted into a feature map by a scale-embedded encoder. In our experiments, the undersampled images fed into the encoder are in two types: the multi-channel images are pre-combined to a single image using sums of squares, and the multi-channel images are not pre-combined. Simultaneously, the 2D voxel coordinates  $(x, y)$  of the MR image grid are transformed into higher-dimension vectors. The feature vectors and the coordinate vectors are concatenated at each coordinate and fed into an MLP to recover voxel intensities at each corresponding coordinate. During training, the encoder and MLP are simultaneously optimized by minimizing the L1 loss between  $I^*$  and  $I_{\theta}$ .

The convolutional encoder network consists of five scale-embedded residual blocks. Each convolutional layer within these blocks uses 5x5-sized kernels to achieve a large receptive field and generates 64 feature channels. We apply the group normalization [21] and use the SWISH [22] as our activation function. The positional encoding dimension  $2L$  is set to 256, while the dimension  $d$  of feature vectors is 128. For MLP, the network has eight fully connected layers. A SWISH activation follows all layers but the last. Besides, we include two skip connections that concatenate the input of the network to the 4th and 7th layers, respectively. Except that there are  $2L + d$ ,  $2L + d + 256$ , and  $2L + d + 256$  neurons in the 1st, 4th, and 7th layers, others have all 256 neurons.

## 3 Experiments and Results

### 3.1 Implementation Details

All our experiments were implemented on a workstation with 64GB RAM and two NVIDIA GeForce RTX 2080 Ti graphics cards. PyTorch 1.8.1 was used as the back end. We trained our model for 100000 iterations using the ADAM optimizer with  $\beta_1 = 0.9, \beta_2 = 0.99$ , and set the batch size to 2. The initial learning rate was set to 0.001 and dropped by half every 10000 iterations.

### 3.2 Dataset Description

In this study, two types of MRI data from the fastMRI dataset [25] were used. One type is the fully-sampled 15-channel knee k-space data, which was acquired

**Table 1.** Quantitative comparison with other parallel reconstruction methods on the fastMRI dataset (**Best** and Second Best).

	Brain		
	$s = 4$	$s = 5$	$s = 6$
GRAPPA [3]	0.8876/36.8103	0.8443/35.5809	0.7921/33.1173
RAKI [23]	0.9501/ <u>39.4045</u>	0.9415/38.1688	0.8942/35.0135
rRAKI [24]	0.9317/38.9997	0.9222/38.0567	0.8450/33.9112
Feng <i>et al.</i> [17]	N/A	N/A	N/A
Ours (with pre-combination)	<u>0.9543/37.7673</u>	<u>0.9624/39.1054</u>	<u>0.9461/36.8490</u>
Ours (without pre-combination)	<b>0.9641/40.5916</b>	<b>0.9664/40.9975</b>	<b>0.9559/39.0309</b>
	Knee		
	$s = 4$	$s = 5$	$s = 6$
GRAPPA [3]	0.7513/32.7750	0.6854/31.4585	0.7930/34.2945
RAKI [23]	0.9169/36.7898	0.8782/34.7770	0.8642/34.3090
rRAKI [24]	0.8440/35.2438	0.7769/32.6516	0.7739/32.3304
Feng <i>et al.</i> [17]	0.9321/ <u>39.4900</u>	0.9296/ <u>39.0400</u>	N/A
Ours (with pre-combination)	<u>0.9480/39.4207</u>	<u>0.9406/38.8031</u>	<u>0.9532/39.8919</u>
Ours (without pre-combination)	<b>0.9532/40.1727</b>	<b>0.9458/39.5118</b>	<b>0.9557/40.3630</b>

using the 2D turbo spin-echo sequence without fat suppression. The other one is the fully-sampled T2-weighted 16-channel brain k-space data with 3T field strength. In our case, the oversampled region of the raw data in the image domain has been removed. All selected datasets were uniformly undersampled with different reconstruction scales, and 8% of the central region was reserved as auto-calibration signal (ACS) lines.

### 3.3 Experimental Results

In our experiments, we compared the proposed method with GRAPPA [3], RAKI [23], residual RAKI (rRAKI) [24], and Feng *et al.* [17] on two datasets with reconstruction scales of 4, 5, and 6. RAKI and rRAKI were trained with identical datasets, scale factors and ACS sizes as the proposed method. The source code and trained network of Feng *et al.* were not publicly available. However, this network was also trained with identical datasets and scale factors, and very close ACS sizes. Therefore, the results reported by Feng *et al.* are used for comparison in this paper. Table 1 shows the quantitative evaluation results. We observe that the proposed method with pre-combination of multi-channel images is significantly superior to all comparison methods, and the results of the proposed method without the pre-combination are further improved.

Fig. 2 visualizes the reconstruction effects of different methods on the three undersampling scales of the brain dataset. We can observe that these GRAPPA-reconstructed MR images are heavily noisy and suffer from obvious artifacts at higher reconstruction scales. In contrast, RAKI’s results have low noise levels and significantly improved SSIM and PSNR; however, the artifacts remain a serious unresolved problem. The performance of rRAKI, including the quality of

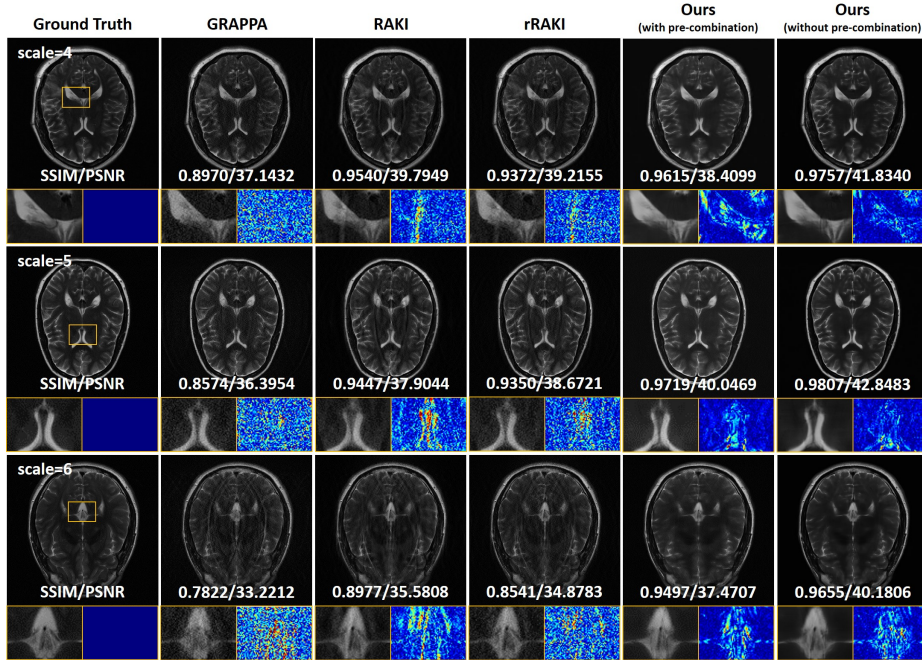


**Fig. 2.** Comparison of the qualitative performance of the proposed method and GRAPPA, RAKI, and rRAKI on brain images of the fastMRI dataset.

the reconstructed images and the evaluation metrics, is between GRAPPA and RAKI. The reconstruction effect of the three methods decreases sharply with increasing undersampling scale. On the contrary, the proposed method is more robust, produces similar image quality at different undersampling scales without noise and obvious artifacts, and outperforms the compared methods.

The reconstruction results of different methods on the knee dataset are depicted in Fig. 3. Similarly to the findings of the brain dataset experiments, GRAPPA, RAKI, and rRAKI continue to exhibit artifacts and noise. Notably, RAKI and rRAKI generate particularly blurry images with overly smoothed tissue boundaries. In contrast, our proposed method successfully reduces noise and artifacts evident in the results of the compared methods and restores images with high-definition detail and improved image contrast, as illustrated by the zoomed-in images in Fig. 3.

## 4 Conclusion

In this paper, we propose an INR-based parallel imaging reconstruction framework. Instead of learning the mapping from undersampled to fully-sampled MRI under a fixed reconstruction scale directly, we propose to learn a continuous implicit neural voxel function, which takes the higher-dimensional coordinate

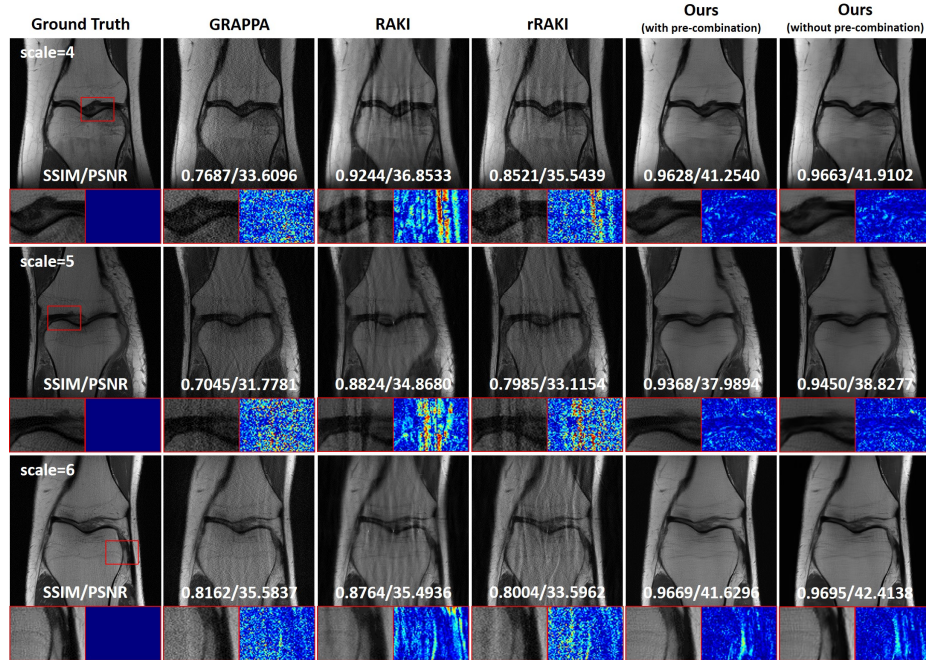


**Fig. 3.** Comparison of the qualitative performance of the proposed method and GRAPPA, RAKI, and rRAKI on knee images of the fastMRI dataset.

vectors and the scale-independent voxel-specific features generated by a convolutional scale-embedded encoder network as input to recover voxel intensities at each corresponding coordinate, thereby restoring high-quality MRI. Once the network training for the proposed method is completed, it does not restrict the application to a specific subject or undersampling scale for parallel MRI imaging reconstruction. Our experimental results conducted on three different reconstruction scales show that the proposed method generates images with higher evaluation metrics and enhanced visual quality compared to the baseline models, making it potential for further accelerating the acquisition of MRI.

Despite the superior quality of the parallel MRI reconstruction, we acknowledge some limitations with our method. Firstly, the experiments in this paper only verify our model with three different undersampling scales. In future studies, more scales of MRI reconstruction and more types of MRI data are expected. Furthermore, the proposed method was trained in a supervised manner and relied on fully-sampled and undersampled image pairs, which are difficult to obtain in real clinics [26,27]. Therefore, an unsupervised approach based on the proposed method remains to be investigated.

## References

1. Michael Lustig, David Donoho, and John M Pauly, “Sparse MRI: The application of compressed sensing for rapid mr imaging,” *Magnetic Resonance in Medicine: An Official Journal of the International Society for Magnetic Resonance in Medicine*, vol. 58, no. 6, pp. 1182–1195, 2007.
2. Klaas P Pruessmann, Markus Weiger, Markus B Scheidegger, and Peter Boesiger, “SENSE: Sensitivity encoding for fast mri,” *Magnetic Resonance in Medicine: An Official Journal of the International Society for Magnetic Resonance in Medicine*, vol. 42, no. 5, pp. 952–962, 1999.
3. Mark A Griswold, Peter M Jakob, Robin M Heidemann, Mathias Nittka, Vladimir Jellus, Jianmin Wang, Berthold Kiefer, and Axel Haase, “Generalized auto-calibrating partially parallel acquisitions (GRAPPA),” *Magnetic Resonance in Medicine: An Official Journal of the International Society for Magnetic Resonance in Medicine*, vol. 47, no. 6, pp. 1202–1210, 2002.
4. Gushan Zeng, Yi Guo, Jiaying Zhan, Zi Wang, Zongying Lai, Xiaofeng Du, Xiaobo Qu, and Di Guo, “A review on deep learning mri reconstruction without fully sampled k-space,” *BMC Medical Imaging*, vol. 21, no. 1, pp. 195, 2021.
5. Shanshan Wang, Zhenghang Su, Leslie Ying, Xi Peng, Shun Zhu, Feng Liang, Dagan Feng, and Dong Liang, “Accelerating magnetic resonance imaging via deep learning,” in *2016 IEEE 13th international symposium on biomedical imaging (ISBI)*. IEEE, 2016, pp. 514–517.
6. Mehmet Akçakaya, Steen Moeller, Sebastian Weingärtner, and Kâmil Uğurbil, “Scan-specific robust artificial-neural-networks for k-space interpolation (RAKI) reconstruction: Database-free deep learning for fast imaging,” *Magnetic Resonance in Medicine*, vol. 81, no. 1, pp. 439–453, 2019.
7. Hemant K Aggarwal, Merry P Mani, and Mathews Jacob, “MoDL: Model-based deep learning architecture for inverse problems,” *IEEE transactions on medical imaging*, vol. 38, no. 2, pp. 394–405, 2018.
8. Jian Sun, Huibin Li, Zongben Xu, et al., “Deep admm-net for compressive sensing mri,” *Advances in neural information processing systems*, vol. 29, 2016.
9. Zhiqin Chen and Hao Zhang, “Learning implicit fields for generative shape modeling,” in *Proceedings of the IEEE/CVF Conference on Computer Vision and Pattern Recognition*, 2019, pp. 5939–5948.
10. Amirali Molaei, Amirhossein Aminimehr, Armin Tavakoli, Amirhossein Kazerouni, Bobby Azad, Reza Azad, and Dorit Merhof, “Implicit neural representation in medical imaging: A comparative survey,” in *Proceedings of the IEEE/CVF International Conference on Computer Vision*, 2023, pp. 2381–2391.
11. Ben Mildenhall, Pratul P Srinivasan, Matthew Tancik, Jonathan T Barron, Ravi Ramamoorthi, and Ren Ng, “Nerf: Representing scenes as neural radiance fields for view synthesis,” *Communications of the ACM*, vol. 65, no. 1, pp. 99–106, 2021.
12. Qing Wu, Yuwei Li, Lan Xu, Ruiming Feng, Hongjiang Wei, Qing Yang, Boliang Yu, Xiaozhao Liu, Jingyi Yu, and Yuyao Zhang, “IREM: High-resolution magnetic resonance image reconstruction via implicit neural representation,” in *Medical Image Computing and Computer Assisted Intervention—MICCAI 2021: 24th International Conference, Strasbourg, France, September 27–October 1, 2021, Proceedings, Part VI 24*. Springer, 2021, pp. 65–74.
13. Zixuan Chen, Jianhuang Lai, Lingxiao Yang, and Xiaohua Xie, “CuNeRF: Cube-based neural radiance field for zero-shot medical image arbitrary-scale super resolution,” *arXiv preprint arXiv:2303.16242*, 2023.

14. Julian McGinnis, Suprosanna Shit, Hongwei Bran Li, Vasiliki Sideri-Lampretsa, Robert Graf, Maik Dannecker, Jiazhen Pan, Nil Stolt-Ansó, Mark Mühlau, Jan S Kirschke, et al., “Single-subject multi-contrast mri super-resolution via implicit neural representations,” in *International Conference on Medical Image Computing and Computer-Assisted Intervention*. Springer, 2023, pp. 173–183.
15. Liyue Shen, John Pauly, and Lei Xing, “NeRP: implicit neural representation learning with prior embedding for sparsely sampled image reconstruction,” *IEEE Transactions on Neural Networks and Learning Systems*, 2022.
16. Junshen Xu, Daniel Moyer, Borjan Gagoski, Juan Eugenio Iglesias, P Ellen Grant, Polina Golland, and Elfar Adalsteinsson, “NeSVoR: Implicit neural representation for slice-to-volume reconstruction in mri,” *IEEE Transactions on Medical Imaging*, 2023.
17. Ruimin Feng, Qing Wu, Yuyao Zhang, and Hongjiang Wei, “A scan-specific unsupervised method for parallel mri reconstruction via implicit neural representation,” in *2023 IEEE 20th International Symposium on Biomedical Imaging (ISBI)*. IEEE, 2023, pp. 1–5.
18. Junwei Yang and Pietro Liò, “Unsupervised adaptive implicit neural representation learning for scan-specific mri reconstruction,” *arXiv preprint arXiv:2312.00677*, 2023.
19. Eric Z Chen, Chi Zhang, Xiao Chen, Yikang Liu, Terrence Chen, and Shanhui Sun, “Computationally efficient 3d mri reconstruction with adaptive mlp,” in *International Conference on Medical Image Computing and Computer-Assisted Intervention*. Springer, 2023, pp. 195–205.
20. Matthew Tancik, Pratul Srinivasan, Ben Mildenhall, Sara Fridovich-Keil, Nithin Raghavan, Utkarsh Singhal, Ravi Ramamoorthi, Jonathan Barron, and Ren Ng, “Fourier features let networks learn high frequency functions in low dimensional domains,” *Advances in Neural Information Processing Systems*, vol. 33, pp. 7537–7547, 2020.
21. Yuxin Wu and Kaiming He, “Group normalization,” in *Proceedings of the European conference on computer vision (ECCV)*, 2018, pp. 3–19.
22. Prajit Ramachandran, Barret Zoph, and Quoc V Le, “Swish: A self-gated activation function,” *arXiv preprint arXiv:1710.05941*, vol. 7, no. 1, pp. 5, 2017.
23. Mehmet Akçakaya, Steen Moeller, Sebastian Weingärtner, and Kâmil Uğurbil, “Scan-specific robust artificial-neural-networks for k-space interpolation (RAKI) reconstruction: Database-free deep learning for fast imaging,” *Magnetic resonance in medicine*, vol. 81, no. 1, pp. 439–453, 2019.
24. Chi Zhang, Steen Moeller, Omer Burak Demirel, Kâmil Uğurbil, and Mehmet Akçakaya, “Residual RAKI: A hybrid linear and non-linear approach for scan-specific k-space deep learning,” *NeuroImage*, vol. 256, pp. 119248, 2022.
25. Florian Knoll, Jure Zbontar, Anuroop Sriram, Matthew J. Muckley, Mary Bruno, Aaron Defazio, Marc Parente, Krzysztof J. Geras, Joe Katsnelson, Hersh Chandarana, Zizhao Zhang, Michal Drozdzal, Adriana Romero, Michael Rabbat, Pascal Vincent, James Pinkerton, Duo Wang, Nafissa Yakubova, Erich Owens, C. Lawrence Zitnick, Michael P. Recht, Daniel K. Sodickson, and Yvonne W. Lui, “fastMRI: A publicly available raw k-space and dicom dataset of knee images for accelerated mr image reconstruction using machine learning,” *Radiology: Artificial Intelligence*, vol. 2, no. 1, pp. e190007, 2020, PMID: 32076662.
26. Jianan Liu, Hao Li, Tao Huang, Euijoon Ahn, Adeel Razi, and Wei Xiang, “Unsupervised representation learning for 3d mri super resolution with degradation adaptation,” *arXiv preprint arXiv:2205.06891*, 2022.

27. Yusheng Zhou, Hao Li, Jianan Liu, Zhengmin Kong, Tao Huang, Euijoon Ah, and Zhihan Lv, “UNAEN: Unsupervised abnormality extraction network for mri motion artifact reduction,” *arXiv preprint arXiv:2301.01732*, 2023.